

1
2
3
4
5
6
7
8
9
10
11
12
13
14
15
16
17
18
19
20
21
22
23
24
25
26
27
28
29
30
31
32
33

Assessing heat exposure to extreme temperatures in urban areas using the Local Climate Zones classification

Joan Gilabert^{1,2,3}, Anna Deluca⁴, Dirk Lauwaet⁵, Joan Ballester⁴, Jordi Corbera², Maria Carmen Llasat¹

¹GAMA Team Department of Applied Physics - University of Barcelona,
²Institute Cartographic and Geological of Catalonia (ICGC),
³URBAG research team, Sostenipra SGR 1412 ICTA-UAB,
⁴Climate and Health Program - Barcelona Institute for Global Health,
⁵Flemish Institute for Technological Research (VITO)

Correspondence to: Joan Gilabert (jgilabert@meteo.ub.edu)

Abstract. Trends of extreme temperature episodes in cities are increasing (in frequency, magnitude and duration) due to regional climate change in interaction with the urban effects. Urban morphologies and thermal properties of the materials used to build them are factors that influence the spatial and temporal climate variability and becomes one of the main reasons for the climatic singularity of cities. This paper presents a methodology to evaluate the urban and peri-urban effect on extreme temperatures exposure in Barcelona (Spain), using the Local Climate Zone (LCZ) classification as a base statement, that allows the comparison with other cities of the world characterized using this criterion. LCZs were introduced as input of the high resolution UrbClim model (100 m spatial resolution) to create the daily temperatures (median and maximum) series for summer (JJA) during the period 1987 to 2016, pixel by pixel, in order to create a cartography of extremes. Using the relationship between mortality due to high temperatures and the temperature distribution, the heat exposure of each LCZ was obtained. Methodological results of the paper show the improvement obtained when LCZs were mapped through a combination of two techniques (from Land Cover/Land Use maps and from WUDAPT method), as well as proposes a methodology to obtain the exposure to high temperatures of different LCZs on urban and peri-urban areas. In the case of Barcelona, the distribution of temperatures for the 90th percentile (about 3-4°C above the average conditions) leads to an increase in the relative risk of mortality of 80%.

34 **1. Introduction**

35 Alterations to the natural environment associated with urban activity mean that climate
36 variability in urban landscapes is more complex than in peri-urban and rural areas. Urban
37 landscapes are home to more than half the world's population and projections show that
38 two-thirds of the world's population will live in cities by 2050 (UN, 2015). Urban areas
39 are certainly more exposed and vulnerable to the negative effects of climate change due
40 to their non-sustainable relationship with surrounding areas and environments. The Urban
41 Climate Change Research Network's Second Assessment Report on Climate Change in
42 Cities (ARC 3.2) (Rosenzweig et al., 2018), places the average annual temperature
43 increase ratio per decade between 0.1 and 0.5°C in the period from 1961 to 2010 in the
44 cities analysed it. And it is estimated that the temperature will rise between 1.3 and 3°C
45 towards the middle of the 21st century (2040-2070) and 1.7 to 4.9°C towards the end
46 (2070-2100).

47 Urban landscapes are particularly sensitive to rising temperatures at all timescales
48 (Pachauri RK et al., 2014). Heat waves (HW) are one of the deadliest weather events
49 and their frequency, intensity and duration are expected to increase in the future due to
50 climate change (Li and Bou-Zeid, 2013; De Jarnett and Pittman, 2017; Sheridan and
51 Dixon, 2016) and the urban heat island (UHI) effect. Consequently, the related health
52 impacts are of emerging environmental health concern (Wolf and McGregor, 2013). In
53 Europe, the growing urbanisation along with the impacts of the increasing of extreme
54 temperature causes increased heat-related mortality (Smid et al., 2019; Ingole et al.,
55 2020).

56 There are many factors that influence the spatial and temporal climate variability in urban
57 areas, such as different urban morphologies and the thermal properties of the materials
58 used to build them (Geletič et al., 2016; Li et al., 2016). One of the main topics usually
59 studied to characterise the urban climate are the extreme temperatures in cities due to UHI
60 effect, which was first discussed back in the 1940s (Balchin and Pye, 1947). Historically,
61 a considerable body of research has been published on the phenomenon (i.e, Oke, 1982;
62 Lo et al., 1997; Arnfield, 2003; Voogt and Oke, 2003; Chen et al., 2006; Mirzaei and
63 Haghghat, 2010; Giannaros et al., 2014; Lehoczky et al., 2017; Sobrino and Irakulis,
64 2020). However, certain methodological inconsistencies have been revealed when
65 comparing different urban climate studies. One of the main reasons is the lack of

66 standardisation to compare the properties that affect specific urban thermal behaviour
67 (Stewart, 2011). Moving forward from this premise, a new methodology based on the
68 Urban Climate Zones defined by Oke (2004) and called Local Climate Zone (LCZ)
69 classification has emerged (Stewart and Oke, 2012). LCZ establishes a system of
70 standardisation for urban and rural areas and their thermal responses. LCZ proposes a
71 classification with a total of 17 measurable categories based on a combination of
72 geometric, thermal, radiative and metabolic parameters that characterise urban and peri-
73 urban areas. By using this classification, it is possible to study the effects of urban climate
74 in more spatial and temporal detail (Bechtel et al., 2015). The combination of built
75 environment (Benzie et al., 2011; Inostroza et al., 2016) is well encompassed by the LCZ
76 approach, and, along with socio-demographic factors (Nayak et al., 2018), this allows us
77 to develop a geospatial distribution of heat exposure (Dickson et al., 2012; Drobinski et
78 al., 2014). Along the same line of research, the international project called World Urban
79 Database and Access Portal Tools (WUDAPT) has created a portal with guidelines based
80 on earth observation data, with the aim of building a worldwide database of cities, using
81 the LCZ classification. This standardisation will allow comparisons between cities, while
82 providing better data for meteorological and climate models (Brousse et al., 2016; Ching
83 et al., 2018). Currently, the available, validated layer for Barcelona on the WUDAPT
84 portal is the one made in our studio to fill in the Metropolitan Area of Barcelona (AMB),
85 as explained in more detail in section 3.1.

86 Due to LCZ classification was originally designed to mainly describe the thermal
87 characteristics of the different land covers and land uses, it is useful to be applied to
88 estimate the level of heat exposure (Vicedo-Cabrera et al., 2014; Lowe et al., 2015;
89 Achebak et al., 2019) to adverse climate conditions that is one of the main goals of this
90 paper. There are a wide range of definitions for the term ‘vulnerability’ (UNISDR, 2009;
91 Cutter, 1996; Llasat et al., 2009), which depend on different physical and social factors
92 (Cutter et al., 2000; Tromeur et al., 2012; Nakamura and Llasat, 2016). In this framework
93 heat vulnerability is understood as a combination of heat exposure (based on high
94 temperatures) and sensitivity (Wolf and McGregor, 2013; Bao et al., 2015; Inostroza et
95 al. 2016), where the last is related with the population characteristics and coping
96 capacities. Although there are some publications that study risk on an urban scale for
97 extreme heat events (Xu et al., 2012; Weber et al., 2015; Krstic et al., 2017; Eum et al.,
98 2018), few have been studied from an LCZ perspective. This paper therefore aims to

99 assess heat exposure using the LCZ classification in a coastal Mediterranean metropolitan
100 region. Barcelona constitutes a good example of a Mediterranean coastal megacity (port
101 cities with a population greater than 1 million in 2005) (Hanson et al., 2011) that can be
102 severely affected by climate change impacts. In effect, annual mean temperature increase
103 in the Mediterranean Basin is higher than the world average (1.5°C above 1880-1899 in
104 2018) and could be above 2.2°C in 2040 without additional mitigation (Lionello et al.,
105 2014; Cramer et al., 2018; MedECC, 2019). Direct impacts on health produced by the
106 frequency and intensity increase of heat waves and tropical nights will be amplified by
107 the urban heat island effect, particularly important in Barcelona (Baccini et al, 2011;
108 Martin-Vide and Moreno, 2020). Associated to this temperature increase, by 2050, for
109 the lower sea-level rise scenarios and current adaptation measures, cities in the
110 Mediterranean will account for half of the 20 global cities with the highest increase in
111 average annual damages (Hallegate et al., 2013).

112 This study is a starting point for new research lines with three objectives in mind: a)
113 making changes to urban land cover and observing the changes in heat exposure to high
114 temperatures without having to resort to climate modelling; b) downscaling the
115 temperature outputs of urban models to resolutions under 100m using the LCZ maps; c)
116 applying this methodology to climate change scenarios.

117 **2. Data and Methods**

118 **2.1. Study area**

119 The Metropolitan Area of Barcelona (AMB) and its surroundings have been selected to
120 apply the LCZ classification. AMB involves the city of Barcelona and 35 adjoining
121 municipal areas (Fig. 1). The AMB is situated in the northwest of the Mediterranean basin
122 and covers an area of 636 km² with a population of around 3.2 million. The city of
123 Barcelona (~1.6 million) is in its centre, between the Llobregat River (South), the Besòs
124 River (North), the Catalan Coastal Range (West) and the Mediterranean Sea (East) (Fig.
125 1b).

126 The Barcelona municipality has been selected to analyse the effect of high temperatures
127 and apply the proposed methodology approach on a neighbourhood scale. Barcelona is
128 divided into 10 districts, which are subdivided into 73 neighbourhoods. It covers an area

129 of 101 km² and has a population density of over 15,000 inh./km², which is higher than
130 New York City, Tokyo or New Delhi. In terms of climate, Barcelona and its surroundings
131 are characterised by hot summers (25°C-27°C average temperature), and the thermal
132 stress of high temperatures is accentuated by the proximity of the sea, which results in a
133 humid atmosphere. Total precipitation in Barcelona is around 600 mm per year. Autumn
134 is the wettest season and has a highly irregular distribution of precipitation, in many cases
135 causing episodes of urban flooding (Gilabert and Llasat, 2017; Cortès et al., 2018).

136

137 **2.2 Methodology design**

138 In order to carry out this study, we followed the workflow shown below:

- 139 1. LCZ Mapping: A GIS methodology based on Land Cover and Land Use (LCLU)
140 maps has been applied to the entire AMB to improve the precision of the
141 international WUDAPT method. The WUDAPT method has been also applied to
142 all the area showed in Figure 1b, both inside and outside AMB, that will be used
143 as input of the climate model.
- 144 2. Climate characterisation of the median and extreme temperature distribution in
145 Barcelona from the outputs of UrbClim model.
- 146 3. Defining the heat exposure thresholds based on the epidemiological temperature-
147 mortality model proposed by Achebak et al. (2018).
- 148 4. Developing a methodology for the thermal characterisation of the LCZs and its
149 assessment.

150 Each one of these steps will be explained in detail in the following sections in order to
151 simplify the understanding of this methodology in which each part is based in the results
152 of the previous one. The own methodology followed constitutes a result of this work.

153 **2.3. LCZ mapping**

154 **2.3.1 Data from official thematic cartography, satellite images and weather stations**

155 In order to create the LCZ cartography data showed in Table 1 have been used. The LCZs
156 were represented following two methods, as explained in section 3. The Land Cover Land

157 Use method was based on using all the layers presented in Table 1, except for the Landsat
158 8 image, which was only used with the WUDAPT methodology and the orthophoto to
159 make the training areas.

160 **2.3.2 Land Cover and Land Use method and WUDAPT method**

161 There are several proposals for mapping LCZs, whether from a bottom up or top down
162 approach (Brousse et al., 2016; Lelovics et al., 2014; Wang et al., 2017; Mitraka et al.,
163 2015). Each LCZ is defined by 10 variables (geometric, radiative and metabolic), which
164 were tested and standardised by Stewart and Oke (2012) and are applied in this study.

165 Our study features a LCZ map that combines two different mapping techniques (Fig. 2).
166 For the administrative region of the AMB (with a more extensive and detailed source of
167 data), a methodology based on land cover and land use (LCLU) data was used that departs
168 from the reclassification of the land use key for the existing high-resolution maps. The
169 LCLU data were combined with LIDAR data, which allowed us to define the height of
170 the buildings. There are other techniques that use similar methodologies to show LCZs,
171 like those by Geletič and Lehnert (2016) or Skarbit et al. (2017). For the area outside the
172 AMB, the international WUDAPT methodology was used, based on satellite earth
173 observation data (Bechtel et al, 2015). This study improved accuracy through a population
174 map and high resolution orthophotos provided by the Cartographic and Geological
175 Institute of Catalonia (ICGC). Both methodologies are summarized below.

176 The LCLU method is based on different Land Cover and Land Use maps (see Table 1),
177 such as the Land Cover Map of Catalonia (LCLU-Cat), which uses an extensive
178 classification of up to 241 categories (CREAF, 2010), and the Urban Atlas (UA) (EEA,
179 2010). The first thematic map was used to define the Land Cover Types and density of
180 vegetation. The UA distinguishes 20 categories of urban areas and discerns between urban
181 fabric type and density, which is why it is very useful for the first 10 categories of LCZ.
182 Each LCLU category corresponds to one of the descriptions of the different
183 morphological parameters that define the LCZ. The Building Heights is another layer of
184 the map, and was made with a LIDAR sensor, which was also used to discern between
185 the different building types of each LCZ.

186 Figure 3 shows the difference between the total coverage of each LCZ when obtained
187 from the LCLU and from WUDAPT maps in AMB (Fig. 2). In the WUDAPT approach,
188 52.8% of the surface area of the AMB consists of urban areas (LCZ 1-10 and E), while
189 in the high-resolution map (LCLU approach), the same type of coverage occupies just
190 37.3%. It is a consequence of the difference in the LCZ characterization processes that
191 both methods follow. Although 17 LCZs are distinguished in the two methods, WUDAPT
192 uses the spectral radiance provided by satellite images and applies a supervised
193 classification based on a random forest generalization method based on training zones
194 (Bechtel et al. 2015). On the contrary, the method LCLU proposed here analyses the
195 intrinsic variables that characterizes each category of LCZ and consequently it has major
196 integrity and quality. It is to say, it has a better resolution. In both methods, we can see
197 that the natural forest category (LCZ-A) is the most common, accounting for 24.1% and
198 18.4% of the land respectively. This is due to the fact that the Metropolitan Area of
199 Barcelona includes Collserola Natural Park in the Coastal Mountain Range. The next
200 most common class is LCZ-C, which corresponds to scrubland and bush. Dealing with
201 land classified as urban, the most common types include industrial estates (LCZ-8), areas
202 with dense buildings less than 25 m tall (LCZ-2) and category LCZ-6, which consists of
203 open arrangements of mid-rise buildings. The WUDAPT map suffers from a lack of
204 characterisation of urban areas, which is not the case for the LCLU map.

205 The resulting LCZ map is a high resolution thematic/vector map/base map (Figure 2b),
206 in which each polygon that makes up the urban fabric is attributed to an LCZ category
207 (Gilabert et al., 2016). Finally, it was rasterised at a resolution of 100 m, applying an all
208 shape filter, so that it could be used as an input for the UrbClim model. The method we
209 followed is shown in the workflow diagram (Figure 4). There are similar examples in the
210 literature, such as the LCZ map for the Île-de-France (www.institutparisregion.fr), or the
211 LCZ-LCLU Map of Vienna (Hammerberg et al., 2018).

212 The WUDAPT method (Bechtel et al., 2015) allows us to create a 100 m x 100 m raster
213 map based on earth observation data from remote sensing. The representative regions of
214 interest are chosen for proposed LCZ categories from earth observation satellite data, with
215 the use of very high resolution aerial orthophotos as a ground truth. The LCZ map, made
216 by the first author of this paper, using the WUDAPT proposal, is officially presented on

217 the project portal and is available for download (www.wudapt.org). This method has been
218 applied to an extended area as is showed at Figure 5.

219 A multi-resolution grid shape file (62.5 m, 125 m and 250 m) containing information on
220 the population as registered in 2016 (IDESCAT, 2018) was used to correct the peri-urban
221 areas of AMB where rural activities cannot see well identified. The orthophoto was used
222 to check and correct any categories and the limits between them.

223 Figure 5 shows the resulting map combining the LCLU method (in raster format) for the
224 administrative region of the AMB, and WUDAPT method for the rest of the study area
225 with a final resolution of 100m.

226 **2.4 Weather stations**

227 Table 2 shows the weather stations within the municipality of Barcelona that have been
228 used to evaluate and compare the characterization of the LCZ with the daily average
229 temperature outputs of the UrbClim model. LCZ and height information are also attached.

230 **2.5 UrbClim model simulation**

231 UrbClim is an Urban Boundary-Layer Climate Model specifically designed to simulate
232 temperature at a very high spatial resolution (here at 100 m; De Ridder et al., 2015). The
233 model consists of a land surface scheme with simplified urban physics coupled to a 3D
234 atmospheric boundary layer. UrbClim is faster than high-resolution mesoscale climate
235 models by at least two orders of magnitude (García-Díez et al., 2016), making the very
236 long runs that are necessary for climate change related studies possible. UrbClim has been
237 recently validated in several European cities, including Barcelona (García-Díez et al.,
238 2016). Currently, within the framework of the Pan-European Urban Climate Service
239 (PUCS) project (H2020, 2017-2010), the urban climate of Barcelona has been modelled
240 until 2100, keeping in mind different Representative Concentration Pathways (RCPs) to
241 observe the consequences of climate change on an urban scale. Barcelona was chosen,
242 among other European cities, and VITO and ISGlobal were the organisations responsible
243 for modelling this city.

244 UrbClim model uses a land-surface and a soil-vegetation-atmosphere transfer scheme that
245 is designed to deal with urban surfaces. Each surface grid cell in the model is made up of

246 portions of vegetation, bare soil and urban surface cover, which are all represented using
247 LCZ mapping. A set of transfer equations, together with appropriate parameter values for
248 albedo, emissivity, aerodynamic and thermal roughness length are used to simulate the
249 heat transfer in each surface grid cell. The large-scale atmospheric conditions are used as
250 lateral and upper boundary conditions. The 3D boundary layer model represents a
251 simplified atmosphere by using the continuity equations for horizontal momentum,
252 potential temperature, specific humidity and mass.

253 The simulations for the 1987-2016 period were used for this period. The UrbClim
254 simulations cover a large domain containing 401x401 horizontal grid points at 100 m
255 resolution (40x40 km approximately), and 19 vertical levels within the lower 3 km of the
256 troposphere. It covers the entire geographical area of the Metropolitan Area of Barcelona,
257 including the neighbouring highly populated cities. The driving model data are updated
258 every 3 hours using ERA-Interim reanalysis (Dee et al., 2011), which runs at a spatial
259 resolution of T255 (approximately 70-80 km). The UrbClim model directly downscales
260 the ERA-Interim reanalysis data to 100 m resolution. The climate distribution of the daily
261 mean temperature (T_{mean}), maximum temperature and dew point temperatures were
262 calculated for all the summer months (JJA). The maximum temperature provides an
263 estimate of the worst conditions that can be expected. It is important for risk management
264 and avoiding heat stroke, which usually occurs during the hours of the day when the
265 temperature reaches its highest value. The dew point temperature (T_{dew}) was used as a
266 starting point to calculate the HUMIDEX Eq. (1) that describes the perceived thermal
267 feeling of a person, by combining the effect of heat and humidity (Masterton and
268 Richardson, 1979). Barcelona has quite a high relative humidity during the summer
269 months, which means that the HUMIDEX increases considerably.

$$270 \quad HUMIDEX = T_{mean} + 0.5555 \left[6.11 e^{5417.7530 \left(\frac{1}{273.16} + \frac{1}{273.15 + T_{dew}} \right)} - 10 \right] \text{ Eq. (1)}$$

271 **2.6 Quantifying heat exposure by temperature**

272 The next step consists of reclassifying the maps of the proposed distributions for the daily
273 mean temperature, keeping in mind the impact that they can have on the health. This was
274 carried out using the results provided in the study by Achebak et al. (2018), in which a
275 distributed lag nonlinear model was used to model the short-term delayed relation

276 between daily summer temperature and mortality data from cardio-respiratory diseases in
277 Barcelona (and 46 other cities), over a similar period of time modelled (Fig. 6). This
278 makes it possible to objectively establish the thresholds for health relative risks (RR),
279 based on temperature. For instance, a RR value of 1.20 means that the relative risk of
280 mortality is 20% higher at a given level of temperature exposure compared to a baseline
281 optimum temperature (e.g. temperature of minimum mortality, when RR=1). Relative
282 risks are statistically significant when the lower bound of the confidence interval is greater
283 than 1.

284 We are assuming that the curve is applicable to all districts of the city (Achebak et al.,
285 2018). Table 3 has been built for RR intervals of 0.2 (20%) following the Figure 6. Each
286 RR interval has been associated to a Heat Exposure Index (HEI) that includes temperature
287 interval based on the curve of Achebak et al. (2018). Barcelona deals with HEI value of
288 1 for temperatures between 18 and 20°C up to a HEI value of 7, for temperatures above
289 31.1°C that would mean a very high relative risk of mortality associated with high
290 temperatures. The use of seven HEI categories has the advantage that it can be applied to
291 any city by adjusting them to the temperature values of that city and to the RR curve
292 considered.

293 **3. Results**

294 **3.1 UrbClim temperature outputs and HEI maps**

295 In order to analyse the impact of the different LCZ in the distribution of high temperatures
296 in summer the maps of maximum and daily mean temperature corresponding to
297 percentiles P50, P75, P90, P95 and P99 have been built (Fig. 7). Barcelona has a high
298 relative humidity due to proximity to the sea that increases the warm perception, and, for
299 this reason, the cartography of the average daily HUMIDEX value has also been
300 represented.

301 As we can see in figure 7, there is a very similar spatial distribution pattern. The lowest
302 temperatures are in the most remote area of the coast and they are mainly associated with
303 categories LCZ A and LCZ 9 (mainly covering areas of woodland or very low-density
304 buildings). A cooling effect can also be noted in the most important parks in the city, as
305 well as on the seafront, because of the sea breeze (the UrbClim model underestimates the

306 sea breeze effect in Barcelona, García-Diez et al., 2016). The highest temperatures can be
307 found in the centre of the city, with a tendency to increase in a north-easterly direction.

308 We saw that P99 of HUMIDEX reached 39°C. In Barcelona, without taking humidity into
309 account, the average temperature in the city can reach above 30°C. Even so, normal
310 temperatures during the summer are around 27°C. In Mediterranean cities, relative
311 humidity is important since it is usually high, a fact that affects temperature (Diffenbaugh
312 et al., 2007). In this sense, we observe that the HUMIDEX can register temperatures of
313 the order of 5°C higher than the sensible temperature. Anyway, this study has focused on
314 sensible temperature because the curve that defines the Heat Exposure Index has been
315 made for sensible temperature. In any case, we must bear in mind that the temperature or
316 heat stress may be higher due to the greater HUMIDEX.

317 Figure 8 shows maps of HEI distribution reclassified the UrbClim output of daily mean
318 temperature according to the proposed thresholds showed in section 2.6. This
319 reclassification turns the extreme temperature maps or hazard maps into heat exposure
320 maps. It can be seen that the HEI is lower in areas with higher altitude and in inter-urban
321 parks (as the Montjuïc Park located in SE of the map), although when P90 is surpassed,
322 the HEI value goes over level 5 for most of the urban fabric. Note that the P50 shows an
323 increase in the relative risk of mortality of 40%.

324 **3.2 Thermal characterisation of the LCZs**

325 In this section we aim to match up each LCZ with a determined thermal behaviour to
326 create a methodology that will allow us to estimate the heat exposure to high temperatures
327 from this data.

328 First, for each climatic percentile (P50, P75, P90, P95 and P99) of daily mean temperature
329 (although it could be also done for maximum temperature and HUMIDEX) we analysed
330 the thermal response of the LCZ (LCZ-T) (Fig. 7). To do it we compared, pixel by pixel,
331 the temperature maps with the LCZ maps and we built a boxplot for each LCZ (Fig. 9).

332 In order to characterise each LCZ we tested its normality and test the differentiate
333 behaviour of each probability density curves adjusted to each LCZ. The results of the
334 normality tests (based on central limit theorem) and comparable variations on the relation
335 between LCZ-T indicated that ANOVA may be used for testing whether the differences

336 in LCZ mean temperatures outlined above are significant or not (Geletic et al., 2016).
337 LCZ C, F and 6 do not follow a normal distribution (at 95%) although they tend to it. This
338 is due to the high thermal variability in these categories. There were statistically
339 significant differences in mean LSTs between most LCZs, but LCZs 4 and 5 were
340 recognized as zones less distinguishable from other LCZs. Once we had the temperature
341 distribution it was possible to map HEI.

342 Transposing the model on LCZ maps allowed us to map heat exposure distributions for
343 Barcelona. This methodology has the advantage that they can be transferred to other cities
344 because it relates each LCZ with a HEI value. It is only need having the LCZ map and
345 knowing some temperature values in the city to calibrate the model. In the case that there
346 would not be a RR-T curve available, it could be applied the same HEI of this paper.

347 Figure 9 shows that LCZ 8 (large low-rise buildings), 1 (compact high-rise), E (asphalt)
348 and 2 (compact mid-rise) (from highest to lowest), have usually the highest temperatures.
349 These LCZ in general terms correspond to the categories with high admittance and high
350 permeability (Stewart and Oke, 2012). In contrast, the lowest temperatures correspond to
351 LCZ 9 (sparsely built), A (dense trees), C (bushes) and G (water), which are wooded areas
352 and parks on the outskirts of the city. On the other hand, crops and bare land (LCZ C and
353 F) show very variable behaviour, as during the day they tend to be surfaces that store and
354 retain heat, while during the night their behaviour registers temperatures under the
355 average of the sample. These surfaces are characterised by a large temperature range
356 given the marked contrast between day and night.

357 Table 4 shows that the more extreme the percentile the larger the standard deviation, as
358 expected. Besides this, the more marked deviations correspond to LCZ C and F, which
359 correspond to wooded or bare areas and which show less thermal inertia. On the other
360 hand, category C is very highly influenced (in the case of Barcelona) by orientation, as
361 there are zones located in shaded parts of valleys while other zones are in the sunny ones,
362 which has a direct impact on the deviation. In the case of category C, we observed that it
363 corresponds to a land use that is not very representative in spatial terms.

364 **3.3 Mapping the heat exposure with LCZs**

365 Figure 10 shows the average behaviour of the LCZs for different temperature percentiles
366 (P50, P75, P90, P95, P99). The values corresponding to range between the 25th and 75th
367 percentiles of each LCZ for each probability scenario have been adjusted to a logarithmic
368 curve that can be very useful to build heat exposure maps for high temperatures based on
369 the thermal properties of the LCZ. Knowing the temperature distribution for each
370 category and scenario allows doing the simulation of the impact on temperature
371 distribution of potential modifications to the urban morphology.

372 As explained in the methodology, seven ranges of temperature have been defined
373 according to different relative risk thresholds (Table 3) established by the curve proposed
374 in the study by Achebak et al. (2018) (Fig. 6). By characterising the LCZ from the model
375 represented in Figure 11, the maps of the Heat Exposure Index associated to high
376 temperatures for different probabilistic scenarios have been built. The scenario
377 corresponding to the P75 of the temperature would imply a ratio of relative risk of
378 mortality increase of 60%, and, 80% in a scenario according to the P90.

379 **3.4 Assessment and comparison of the LCZ-T relationship**

380 The results of the LCZ-T relationship as well as the results of the Urban Climate model
381 (UC) have been compared with the distribution of temperature obtained from series of
382 over 10 years for five weather stations (Table 2) located in different LCZ in the
383 municipality of Barcelona. Root mean square error (RMSE) and the differences between
384 the output of both (UrbClim model and LCZ-T relationship) and observations have been
385 obtained in order to compare the results (Tables 5 and 6). We want to highlight that the
386 UrbClim has been already validated in Barcelona by García-Díez et al. (2016) as outlined
387 in section 2.6. Table 5 shows that differences in absolute value are lower than 1.2°C. In
388 all the cases they are equal or below 0.5 °C for the percentile of 50, and also for the
389 percentile of 75 with the exception of the Raval station, that is placed in the oldest part of
390 the city. It should also be kept in mind that a standalone observation is not the same as an
391 aerial 100 x 100 m observation, and this fact is particularly important when the weather
392 station is surrounded by buildings.

393 The HEI maps drawn up using the LCZs were compared with the map based on
394 temperature distributed created by UrbClim (Table 6). Coincidences between pixels for

395 both models are above 80% for percentiles P50, P75 and P90, and more than 60% in all
396 cases.

397

398 **4. Discussion and conclusions**

399 This paper presents a methodology to characterize the distribution of daily mean
400 temperature in basis to the Local Climate Zones (LCZs) mapping in different temperature
401 scenarios on summer (June-July-August). The climate percentiles have been obtained for
402 the period 1987-2016 and applied at 100 m resolution to the city of Barcelona. Although
403 other authors have already worked with the relationship between thermal behaviour and
404 LCZ category (Stewart et al., 2014; Skarbit and Gal., 2015; Geletič et al., 2016; Verdonck
405 et al., 2018) they have usually applied Land Surface Temperature satellite images, for the
406 summer months and a short time period. Other characterizations of LCZ using weather
407 stations can also be found in Alexander and Mills (2014) and Kotharjar and Bagade
408 (2018). In this case, these authors have worked with climate series from observational
409 data. The advantage of the methodology proposed here, in which the LCZ distribution
410 has been compared with the outputs of a high-resolution climate model (UrbClim) is that
411 the relationship has been established from long climate series and for the entire selected
412 region. Currently, there are multiple studies characterizing LCZs using urban model
413 outputs (Aminipouri et al., 2019; Beck et al., 2018; Geletič et al., 2018; Kwok et al., 2019;
414 Unger et al., 2018), but there are not with climatic outings that span so many years.

415 The results of this methodology applied to the Metropolitan Area of Barcelona have
416 showed a major difference between the thermal response in summer for the different LCZ
417 that this obtained from some satellite images. In terms of land use, LCZ A and C, that
418 belong to the most prevalent categories, show the lowest temperatures, consistent with
419 the majority of studies carried out (e.g. Geletič et al., 2016). In our case, category C
420 shows a wider interquartile range than the other types. This is because this category is
421 found in different altitudes along the Catalan Coastal Range and in areas with different
422 orientations. Regarding category B, attributed to the majority of interurban parks, it
423 maintains temperatures below those of the most typical urban zones.

424 The highest daily mean summer temperatures in Barcelona are concentrated in LCZ 2, E,
425 1, 8 F and 10, with LCZs 2, 1 and E being the most representative of the urban planning
426 in the city centre. With regard to LCZ 8 and 10, these are zones that tend to record high
427 temperatures due to the nature of the activities and materials on the land cover (in the
428 most cases, metal structures). The urban LCZ with the lowest temperatures is 9, which is
429 almost non-existent in Barcelona and is located mainly in zones in the Catalan Coastal
430 Range with a significant altitudinal slope. Another urban LCZ with low relative
431 temperatures commonly found in the city is 6, which is mainly located in the
432 neighbourhoods furthest away from the coast and closer to the mountain. These
433 neighbourhoods have a higher percentage of urban green cover, less dense buildings and
434 one of the highest per capita gross domestic product in the city.

435 The paper has also introduced the Heat Exposure Index (HEI), that evaluates the increase
436 of the risk of mortality ratio as a consequence of heat exposure in basis to the model
437 proposed by Achebak et al. (2018) which connects relative risk of mortality caused by
438 cardio-respiratory failure with the effects of high temperatures. This index, associated to
439 each LCZ once the temperature has been associated to it, allows mapping the HEI. The
440 comparison between the Heat Exposure Index maps elaborated directly from the
441 temperature outputs produced by the UrbClim model and those produced from LCZ
442 cartography is well-suited to simulate them for scenarios corresponding to percentiles of
443 temperature between 50% and 90%, and, in the case in which there is no coincidence
444 between the HEI value in the pixel, it is more usual underestimation than overestimation.
445 In the case of Barcelona, the distribution of temperatures for the P90 (about 3-4°C
446 compared to average conditions) leads to an increase in the relative risk of mortality of
447 80%, and 40% in the case of P50.

448 This paper also provides comparison of two methodologies to cartography the LCZ. The
449 WUDAPT and the Land Cover Land Use (LCLU) method based on land use maps. The
450 international standard method WUDAPT (is exclusively based on satellite earth
451 observation data (Ching et al., 2018). The LCLU departs from land use maps, Urban
452 Atlas, LIDAR measurements and orthophotos. The study area has been mapped using two
453 techniques, the LCLU based on land use maps and the WUDAPT. The LCLU has been
454 applied to the Metropolitan Area of Barcelona and the WUDAPT to the entire region
455 (inside and outside) the AMB. The WUDAPT map suffers from a lack of characterisation

456 of different types of urban areas, which is not the case for the Land Cover Land Use.
457 Then, when the required data is available it is better to apply the LCLU methodology than
458 the WUDAPT one. In this study, the curve of Achebak et al. (2018) was taken into
459 account, as representative of the whole of Barcelona city. In the future, it would be good
460 to have a similar curve for different districts of the city. In addition to this, future work
461 includes mapping the sensitivity taking into account coping capacities based on gross
462 domestic product (GDP), social structure of the neighbourhood, etcetera. This would
463 include vulnerability.

464 In conclusion, the LCZ-T relation based on the characterisation of the average
465 temperature for each LCZ corresponding to different percentile distribution, allows us to
466 consider adaptive methods, proposing changes to more sustainable urban planning, for
467 example the use of green or white cover. The advantage of the proposed methodology is
468 that it allows to obtain a heat exposure distribution for summer temperatures without
469 having to resort climate models, by applying the model of temperature distribution
470 associated to each LCZ. It can be also useful to do different experiments modifying land
471 uses and land coverages over the cartography, and, consequently, the LCZ distribution
472 and their associated Heat Exposure Index. Another possibility is being able to separate
473 the heat exposure levels on an LCZ map with higher spatial resolutions to those used in
474 weather models and climate models.

475 **Acknowledgements**

476 This publication was supported by the Industrial Doctorate Programme (ref. 2015-DI-
477 038) between the University of Barcelona and the Cartographic and Geological Institute
478 of Catalonia, the Water Research Institute (IdRA) at the University of Barcelona, M-
479 CostAdapt (CTM2017-83655-C2-2-R) research projects (MINECO/AEI/FEDER, UE)
480 and ERC Consolidator Grant awarded to Gara Villalba (818002-URBAG). The authors
481 would like to thank the European Environment Agency (EEA), Centre for Ecological
482 Research and Forestry Applications (CREAF) and Metropolitan Area of Barcelona for
483 the land use maps available. We would also like to thank the State Meteorological Agency
484 (AEMET) and the Meteorological Service of Catalonia (SMC) for the weather station
485 data. Finally, we want to thank Hicham for giving us the RR model.

486 JB gratefully acknowledges funding from the European Union's Horizon 2020 research
487 and innovation programme under grant agreements No 865564 (European Research
488 Council Consolidator Grant EARLY-ADAPT), 727852 (project Blue-Action) and
489 730004 (project PUCS), and from the Ministry of Science and Innovation (MCIU) under
490 grant agreements No RYC2018-025446-I (programme Ramón y Cajal) and EUR2019-
491 103822 (project EURO-ADAPT).

492 **Author contributions**

493 JG conceived the study, designed and carried out the data analysis and wrote the paper.
494 MCL, JC and JB have participated in defining the analysis and methodology, contributed
495 to interpreting the results, and to writing the paper. DL and AdL have run the UrbClim
496 model and prepare the output data.

497 **Competing interests**

498 The authors declare that they have no conflict of interest.

499 **References**

500 Achebak, H., Devolder, D., and Ballester, J.: Heat-related mortality trends under recent
501 climate warming in Spain: A 36-year observational study. *PLoS med.* 15(7): e1002617,
502 2018.

503 Achebak, H., Devolder, D., and Ballester, J.: Trends in temperature-related age-specific
504 and sex-specific mortality from cardiovascular diseases in Spain: a national time-series
505 analysis. *The Lancet Planetary Health*, 3(7), e297-e306, 2019.

506 Alexander, P., and Mills, G.: Local climate classification and Dublin's urban heat
507 island. *Atmosphere*. 5(4): 755-774, 2014.

508 Aminipouri, M., Knudby, A. J., Krayenhoff, E. S., Zickfeld, K. and Middel, A.:
509 Modelling the impact of increased street tree cover on mean radiant temperature across
510 Vancouver's local climate zones. *Urban Forestry & Urban Greening*, 39, 9–17, 2019.

511 Arnfield, A. J.: Two decades of urban climate research: a review of turbulence, exchanges
512 of energy and water, and the urban heat island. *Int. J. Climatol.* 23(1): 1-26, 2003.

513 Baccini, M., Kosatsky, T., Analitis, A., Anderson, H.R., D'Ovidio, M., Menne, B.,
514 Michelozzi, P., Biggeri, A.: Impact of heat on mortality in 15 European cities: attributable
515 deaths under different weather scenarios. *J Epidemiol Commun H*, 65, 64-70, 2011.

516 Balchin, W. G. V., and Pye, N.: A micro-climatological investigation of bath and the
517 surrounding district. *Q. J. Royal Meteorol. Soc.* 73(317-318): 297-323, 1947.

518 Bao, J., Li, X. and Yu, C.: The construction and validation of the heat vulnerability index,
519 a review. *Int. J. Environ. Res. Public Health*. 12(7): 7220-7234, 2015.

520 Beck, C., Straub, A., Breitner, S., Cyrus, J., Philipp, A., Rathmann, J., Schneider, A.,
521 Wolf, K. and Jacobeit, J.: Air temperature characteristics of local climate zones in the
522 Augsburg urban area (Bavaria, southern Germany) under varying synoptic conditions.
523 *Urban Climate*, 25, 152–166, 2018.

524 Bechtel, B., Alexander, P. J., Böhner, J., Ching, J., Conrad, O., Feddema, J., Mills, G.,
525 See, L., and Stewart I.: Mapping local climate zones for a worldwide database of the form
526 and function of cities. *ISPRS Int. J. Geo-Inf.* 4(1): 199-219, 2015.

527 Benzie, M., Harvey, A., Burningham, K., Hodgson, N., and Siddiqi, A.: Vulnerability to
528 heatwaves and drought: Case studies of adaptation to climate change in South-west
529 England. Joseph Rountree Foundations, 2011.

530 Brousse, O., Martilli, A., Foley, M., Mills, G., and Bechtel B.: WUDAPT, an efficient
531 land use producing data tool for mesoscale models? Integration of urban LCZ in WRF
532 over Madrid. *Urban Clim.* 17: 116-134, 2016.

533 Chen X. L., Zhao H. M., Li P. X., and Yin Z. Y.: Remote sensing image-based analysis
534 of the relationship between urban heat island and land use/cover changes. *Remote Sens.*
535 *Environ.* 104(2): 133-146, 2006.

536 Ching, J., Mills, G., Bechtel, B., See, L., Feddema, J., Wang, X., Ren, C., Brousse, O.,
537 Martilli, A., Neophytou, M., Mouzoudires, P., Stewart, I., Hanna, A., Ng, E., Foley, M.,
538 Alexander, P., Aliaga, D., Niyogi, D., Shreevastava, A., Bhalachandran, S., Masson, V.,
539 Hidalgo, J., Fung, J., de Fatima Andrad, M., Baklanov, A., Wei Dai, D., Milcinski, G.,
540 Demuzere, M., Brunzell, N., Pesaresi, M., Miao, S., Mu, Q., Chen, F., and Theeuwes, N.:

541 World urban data base and access portal tools (WUDAPT), an urban weather, climate and
542 environmental modelling infrastructure for the Anthropocene. *Bull. Am. Meteorol. Soc.*
543 99(9): 1907-1924, 2018.

544 Cortès, M., Llasat, M. C., Gilabert, J., Llasat-Botija, M., Turco, M., Marcos, R., Martin
545 Vide, J. P., and Falcón L.: Towards a better understanding of the evolution of the flood
546 risk in Mediterranean urban areas: the case of Barcelona. *Nat. Hazards.* 93(1): 39-60,
547 2018.

548 Cutter, S. L.: Vulnerability to environmental hazards. *Prog. Hum. Geogr.* 20(4): 529-539,
549 1996.

550 Cutter, S.L., Mitchell, J. T., and Scott, M. S.: Revealing the vulnerability of people and
551 places: a case study of Georgetown County, South Carolina. *Ann. Am. Assoc.*
552 *Geogr.* 90(4): 713-737, 2000.

553 Cramer, W., Guiot, J., Fader, M., Garrabou, J., Gattuso, J. P., Iglesias, A., Lange, M. A.,
554 Lionello, P., Llasat, M. C., Paz, S., Peñuelas, J., Snoussi, M., Toreti, A., Tsimplis, M. N.,
555 and Xoplaki, E.: Climate change and interconnected risks to sustainable development in
556 the Mediterranean. *Nat. Clim. Change* 8:972-980, doi: 10.1038/s41558-018-0299-2,
557 2018.

558 Dee, D. P., Uppala, S. M., Simmons, A. J., Berrisford, P., Poli, P., Kobayashi, S., Andrae,
559 U., Balmaseda, M. A., Balsamo, G., Bauer, P., Bechtold, P., Beljaars, A. C. M., van de
560 Berg, L., Bidlot, J., Bormann, N., Delsol, C., Dragani, R., Fuentes, M., Geer, A. J., Healy
561 S. B., Hersbach, H., Hólm, E. V., Isaksen, L., Kallberg, P., Kölher, M., Matricardi, M.,
562 McNally, A. P., Morcrette, J. J., Park, B. K., Peubey, C., de Rosnay, P., Tavolato, C.,
563 Thépaut, J. N. and Vitart, F.: The ERA-Interim reanalysis: Configuration and
564 performance of the data assimilation system. *Q. J. Roy. Meteor. Soc.* 137(656): 553-597,
565 2011.

566 DeJarnett, N., and Pittman, M.: Protecting the Health and Wellbeing of Communities in
567 a Changing Climate. *Proceedings of a Workshop – in Brief.* The National Academies
568 Press. 10.17226/24797, 8p, 2017.

- 569 De Ridder, K., Lauwaet, D., and Maiheu, B.: UrbClim–A fast urban boundary layer
570 climate model. *Urban Clim.* 12: 21-48, 2015.
- 571 Dickson, E., Baker, J. L., and Hoornweg, D.: Urban risk assessments: understanding
572 disaster and climate risk in cities. The World Bank Publications, 2012.
- 573 Diffenbaugh, N. S., Pal, J. S., Giorgi, F., and Gao, X.: Heat stress intensification in the
574 Mediterranean climate change hotspot. *Geophysical Research Letters*, 34(11), 2007.
- 575 Drobinski, P., Ducrocq, V., Alpert, P., Anagnostou, E., Béranger, K., Borga, M., Braud,
576 I., Chanzy, A., Davolio, S., Delrieu, G., Estournel, C., Filali Boubrahmi, N., Font, J.,
577 Grubisic, V., Gualdi, S., Homar, V., Ivancan-Picek, B., Kottmeier, C., Kotroni, V.,
578 Lagouvardos, K., Lionello, P., Llasat, M. C., Ludwig, W., Lutoff, C., Mariotti, A.,
579 Richard, E., Romero, R., Rotunno, R., Roussot, O., Ruin, I., Somot, S., Taupier-Letage,
580 I., Tintore, J., Uijlenhoet, R. and Wernli, H.: HyMeX, a 10-year multidisciplinary
581 program on the Mediterranean water cycle, *B. Am. Meteorol. Soc.* 95(7): 1063-1082,
582 2014.
- 583 Eum, J. H., Kim, K., Jung, E. H., and Rho, P.: Evaluation and Utilization of Thermal
584 Environment Associated with Policy: A Case Study of Daegu Metropolitan City in South
585 Korea. *Sustainability.* 10(4): 1179, 2018.
- 586 García Díez, M., Lauwaet, D., Hooyberghs, H., Ballester, J., De Ridder, K., and Rodó,
587 X.: Advantages of using a fast urban boundary layer model as compared to a full
588 mesoscale model to simulate the urban heat island of Barcelona. *Geosci. Model Dev.*
589 9(12): 4439-4450, 2016.
- 590 Geletič, J., Lehnert, M., Dobrovolný, P.: Land Surface Temperature Differences within
591 Local Climate Zones, Based on Two Central European Cities. *Remote Sens.* 8(10): 788,
592 2016.
- 593 Geletič, J., Lehnert, M.: GIS-based delineation of local climate zones: The case of
594 medium-sized Central European cities. *Morav. Geogr. Rep.* 24(3): 2-12, 2016.

595 Geletič, J., Lehnert, M., Savic, S., and Milošević, D.: Modelled spatiotemporal variability
596 of outdoor thermal comfort in local climate zones of the city of Brno, Czech Republic.
597 *Science of the Total Environment*, 624, 385–395, 2018.

598 Giannaros, T. M., Melas, D., Daglis, I. A., and Keramitsoglou, I.: Development of an
599 operational modeling system for urban heat islands: an application to Athens, Greece.
600 *Nat. Hazards Earth Syst. Sci.*, 14(2), 347, 2014.

601 Gilabert, J., Tardà, A., Llasat, M. C., and Corbera, J.: Assessment of Local Climate Zones
602 over Metropolitan Area of Barcelona and added value of Urban Atlas, Corine Land Cover
603 and Copernicus Layers under INSPIRE Specifications. INSPIRE Conference, Barcelona,
604 2016.

605 Gilabert, J., and Llasat, M. C.: Circulation Weather Types associated with extreme flood
606 events in Northwestern Mediterranean. *Int. J. Climatol.* 38(4): 1864-1876, 2017.

607 Hallegatte, S., Green, C., Nicholls, R. J. and Corfee-Morlot, J.: Future flood losses in
608 major coastal cities. *Nat. Clim. Change* 3, 802–806, 2013.

609 Hammerberg, K., Brousse, O., Martilli, A., and Mahdavi A.: Implications of employing
610 detailed urban canopy parameters for mesoscale climate modelling: a comparison
611 between WUDAPT and GIS databases over Vienna, Austria. *Int. J. of Climatol.* 38: 1241-
612 1257, 2018.

613 Hanson, S., Nicholls, R., Ranger, N., Hallegatte, S., Cofree-Morlot, J., Herweijer, C.,
614 Chateau, J.: A global ranking of port cities with high exposure to climate extremes.
615 *Climatic Change*, 104(1), 89-111, 2011.

616 Ingole, V., Mari-Dell’Olmo, M., Deluca, A., Quijal, M., Borrell, C., Rodríguez-Sanz, M.,
617 Achebak, H., Lauwet, D., Gilabert, J., Murage, P., Hajat, S., Basagaña, X., and Ballester,
618 J.: Spatial Variability of Heat-Related Mortality in Barcelona from 1992–2015: A Case
619 Crossover Study Design. *Int. J. Environ. Res. Public Health.* 17(7): 2553, 2020.

620 Inostroza, L., Palme, M., and de la Barrera, F.: A heat vulnerability index: spatial patterns
621 of exposure, sensitivity and adaptive capacity for Santiago de Chile. *PloS one.* 11(9):
622 e0162464, 2016.

623 Kotharkar, R., Bagade, A.: Local Climate Zone classification for Indian cities: A case
624 study of Nagpur. *Urban clim.* 24: 369-392, 2018.

625 Krstic, N., Yuchi, W., Ho, H. C., Walker, B. B., Knudby, A. J., and Henderson, S. B.:
626 The Heat Exposure Integrated Deprivation Index (HEIDI): A data-driven approach to
627 quantifying neighborhood risk during extreme hot weather. *Environ. Int.* 109: 42-52,
628 2017.

629 Kwok, Y. T., Schoetter, R., Lau, K. K. L., Hidalgo, J., Ren, C., Pigeon, G., and Masson,
630 V.: How well does the local climate zone scheme discern the thermal environment of
631 Toulouse (France)? An analysis using numerical simulation data. *International Journal of*
632 *Climatology*, 39(14), 5292-5315, 2019.

633 Lehoczky, A., Sobrino, J. A., Skoković, D., and Aguilar, E.: The Urban Heat Island Effect
634 in the City of Valencia: A Case Study for Hot Summer Days. *Urban Science*, 1(1), 9,
635 2017.

636 Lelovics, E., Unger, J., and Gál, T.: Design of an urban monitoring network based on
637 Local Climate Zone mapping and temperature pattern modelling. *Clim. Res.* 60: 51-62.

638 Li D, Bou-Zeid E. (2013) Synergistic interactions between urban heat islands and heat
639 waves: the impact in cities is larger than the sum of its parts. *J. Appl. Meteorol.*
640 *Clim.* 52(9): 2051-2064, 2014.

641 Li, X., Li, W., Middel, A., Harlan, S. L., Brazel, A. J, and Turner, B. L.: Remote sensing
642 of the surface urban heat island and land architecture in Phoenix, Arizona: Combined
643 effects of land composition and configuration and cadastral- demographic- economic
644 factors. *Remote Sens. Environ.* 174: 233-243, 2016.

645 Lionello, P., Abrantes, F., Gacic, M., Planton, S., Trigo, R., and Ulbrich, U.: The climate
646 of the Mediterranean region: research progress and climate change impacts. *Reg Environ*
647 *Change* 14, 1679–1684., 2014.

648 Llasat, M. C., Llasat-Botija, M., López, L.: A press database on natural risks and its
649 application in the study of floods in Northeastern Spain. *Nat. Hazard. Earth Sys.* 9(6):
650 2049-2061, 2009.

651 Lo C. P., Quattrochi, D. A., and Luvall, J. C.: Application of high-resolution thermal
652 infrared remote sensing and GIS to assess the urban heat island effect. *Int. J. Remote*
653 *Sens.* 18(2): 287-304, 1997.

654 Lowe, R., Ballester, J., Creswick, J., Robine, J. M., Herrmann, F. R., and Rodó, X.:
655 Evaluating the performance of a climate-driven mortality model during heat waves and
656 cold spells in Europe. *International journal of environmental research and public*
657 *health*, 12(2), 1279-1294, 2015.

658 Martin-Vide, J., and Moreno-Garcia, M. C.: Probability values for the intensity of
659 Barcelona's urban heat island (Spain). *Atmos. Res.*, 104877, 2020.

660 Masterton, J. M., and Richardson, F. A.: Humidex: a method of quantifying human
661 discomfort due to excessive heat and humidity. Environment Canada. *Atmospheric*
662 *Environment*, 1979.

663 MedECC.: Risks associated to climate and environmental changes in the Mediterranean
664 region. A preliminary assessment by the MedECC Network. *Science-policy interface –*
665 *2019.* 36 pp, 2019.

666 Mirzaei, P. A., Haghghat, F.: Approaches to study urban heat island–abilities and
667 limitations. *Build. Environ.* 45(10): 2192-2201, 2010.

668 Mitraka, Z., del Frate, F., Chrysoulakis, N., and Gastellu-Etchegorry, J. P.: Exploiting
669 earth observation data products for mapping local climate zones. *Joint Urban Remote*
670 *Sensing Event (JURSE).* 1-4, 2015.

671 Nakamura, I., and Llasat, M. C.: Policy and systems of flood risk management: a
672 comparative study between Japan and Spain. *Nat. Hazards.* 87(2): 919-943, 2017.

673 Nations, United.: *World population prospects: The 2015 revision.* United Nations Econ.
674 *Soc. Aff.* 33(2): 1-66, 2015.

675 Nayak, S. G., Shrestha, S., Kinney, P. L., Ross, Z., Sheridan, S. C., Pantea, C. I., Hsu, W.
676 H., Muscatiello, N., and Hwang, S. A.: Development of a heat vulnerability index for
677 New York State. *Public health.* 161: 127-137, 2018.

678 Oke, T. R.: The energetic basis of the urban heat island. *Q. J. Roy. Meteor. Soc.* 108(455):
679 1-24, 1982.

680 Oke, T.R.: Urban observations, World Meteorological Organization, IOM Report N° 81,
681 WMO/TD n°1250, 2004.

682 Pachauri, R. K., Allen, M. R., Barros, V. R., Broome, J., Cramer, W., Christ, R., Church
683 J. A., Clarke, L., Dahe, Q., Dasgupta, P., Dubash, N. K., Edenhofer, O., Elgizouli, I.,
684 Field, C. B., Forster, P., Friedlingstein, P., Fuglestvedt, J., Gomez-Echeverri, L.,
685 Hallegatte, S., Hegerl, G., Howden, M., Jiang, K., Jimenez Cisneroz, B., Kattsov, K., Lee,
686 H., Mach, K. J., Marotzke, J., Mastrandrea, M. D., Meyer, L., Minx, J., Mulugetta, Y.,
687 O'Brien, Oppenheimer, M., Pereira, J. J., Pichs-Madruga, R., Plattner, G. K., Pörtner, H.
688 O., Power, S. B., Preston, B., Ravindranath, N.H., Reisinger, A., Riahi, K., Rusticucci,
689 M., Scholes, R., Seyboth, K., Sokona, Y., Stavins, R., Stocker, T. F., Tschakert, P., van
690 Vuuren, D., and van Ypserle, J.P.: Climate change 2014: synthesis report. Contribution
691 of working groups I, II and III to the fifth assessment report of the intergovernmental
692 panel on climate change. R. Pachauri, L. Meyer (Eds.), IPCC, Geneva, Switzerland.
693 ISBN: 978-92-9169-143-2, 2014.

694 Rosenzweig, C., Solecki, W. D., Romero-Lankao, P., Mehrotra, S., Dhakal, S., and Ali
695 Ibrahim, S.: Climate change and cities. Second assessment report of the urban climate
696 change research network. New York: Cambridge University Press. Retrieved from:
697 [http://www.cambridge.org/ws/academic/subjects/earth-and-environmental-](http://www.cambridge.org/ws/academic/subjects/earth-and-environmental-science/climatology-and-climate-change/climate-change-and-cities-second-assessment-report-urban-climate-change-research-network)
698 [science/climatology-and-climate-change/climate-change-and-cities-second-assessment-](http://www.cambridge.org/ws/academic/subjects/earth-and-environmental-science/climatology-and-climate-change/climate-change-and-cities-second-assessment-report-urban-climate-change-research-network)
699 [report-urban-climate-change-research-network](http://www.cambridge.org/ws/academic/subjects/earth-and-environmental-science/climatology-and-climate-change/climate-change-and-cities-second-assessment-report-urban-climate-change-research-network), 2018.

700 Sheridan, S. C., and Dixon, P. G.: Spatiotemporal trends in human vulnerability and
701 adaptation to heat across the United States. *Anthropocene*. 20: 61-73, 2016.

702 Skarbit, N., Stewart, I. D., Unger, J., and Gál, T.: Employing an urban meteorological
703 network to monitor air temperature conditions in the 'local climate zones' of Szeged,
704 Hungary. *Int. J. Climatol.* 37: 582-596, 2017.

705 Skarbit, N., Gal, T., and Unger, J.: Airborne surface temperature differences of the
706 different Local Climate Zones in the urban area of a medium sized city. Joint Urban
707 Remote Sensing Event (JURSE). 1-4, 2015.

708 Smid, M., Russo, S., Costa, A. C., Granell, C., and Pebesma, E.: Ranking European
709 capitals by exposure to heat waves and cold waves. *Urban Climate*, 27, 388-402, 2019.

710 Sobrino, J. A., and Irakulis, I.: A Methodology for Comparing the Surface Urban Heat
711 Island in Selected Urban Agglomerations Around the World from Sentinel-3 SLSTR
712 Data. *Remote Sensing*, 12(12), 2052, 2020.

713 Stewart, I. D.: A systematic review and scientific critique of methodology in modern
714 urban heat island literature. *Int. J. Climatol.* 31(2): 200-217, 2011.

715 Stewart, I. D., and Oke, T. R.: Local climate zones for urban temperature studies. *B. Am.*
716 *Meteorol. Soc.* 93(12): 1879-1900, 2012.

717 Stewart, I. D., Oke, T. R., and Krayenhoff, E. S.: Evaluation of the ‘local climate zone’
718 scheme using temperature observations and model simulations. *Int. J. Climatol.* 34(4):
719 1062-1080, 2014.

720 Tromeur, E., Ménard, R., Bailly, J. B., and Soulié, C.: Urban vulnerability and
721 resilience within the context of climate change. *Nat. Hazards Earth Syst. Sci.*, 12(5),
722 2012.

723 Unger, J., Skarbit, N. and Gál, T.: Evaluation of outdoor human thermal sensation of local
724 climate zones based on long-term database. *International Journal of Biometeorology*,
725 62(2), 183–193, 2018.

726 UNISDR, UNOFDRR.: Terminology on disaster risk reduction. Geneva, Switzerland,
727 2009.

728 Verdonck, M. L., Demuzere, M., Hooyberghs, H., Beck, C., Cyrus, J., Schneider, A.,
729 Dewulf, R., and Van Coillie, F.: The potential of local climate zones maps as a heat stress
730 assessment tool, supported by simulated air temperature data. *Landscape Urban plan.*
731 178: 183-197, 2018.

732 Vicedo-Cabrera, A. M., Iñiguez, C., Barona, C., and Ballester, F.: Exposure to elevated
733 temperatures and risk of preterm birth in Valencia, Spain. *Environmental research*, 134,
734 210-217, 2014.

735 Voogt, J. A., and Oke, T. R.: Thermal remote sensing of urban climates Remote Sens.
736 Environ. 86(3): 370-384, 2003.

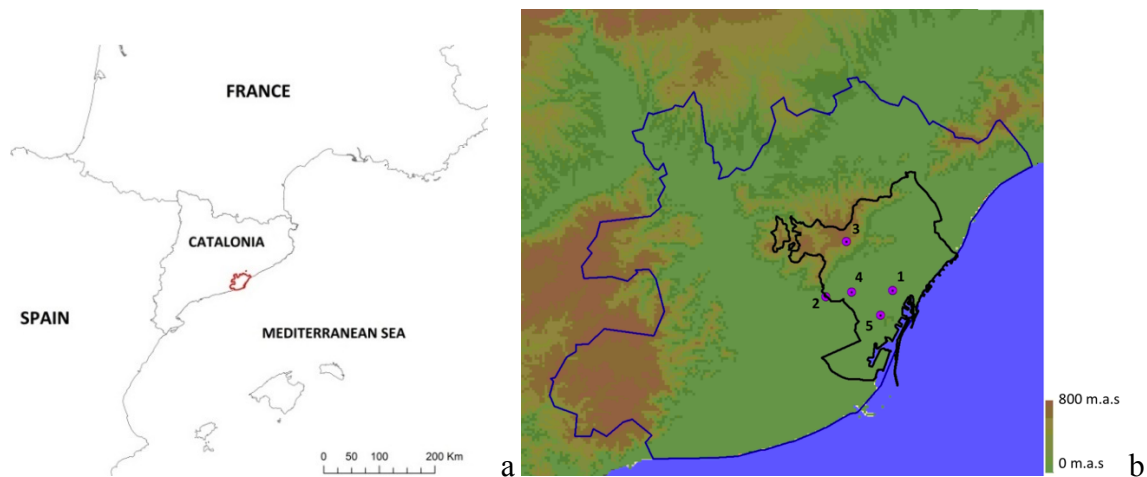
737 Wang, R., Ren, C., Xu, Y., Lau, K. K. L., and Shi, Y.: Mapping the local climate zones
738 of urban areas by GIS-based and WUDAPT methods: A case study of Hong Kong. Urban
739 Clim. 24: 567- 576, 2017.

740 Weber, S., Sadoff, N., Zell, E., and de Sherbinin A.: Policy-relevant indicators for
741 mapping the vulnerability of urban populations to extreme heat events: A case study of
742 Philadelphia. Appl. Geogr. 63: 231-243, 2015, 2015.

743 Wolf, T., and McGregor G.: The development of a heat wave vulnerability index for
744 London, United Kingdom. Weather and Climate Extremes. 1: 59-68, 2013

745 Xu, Z., Sheffield, P. E., Hu, W., Su, H., Yu, W., Qi, X., and Tong S.: Climate change and
746 children's health- A call for research on what works to protect children. I Int. J. Environ.
747 Res. Public Health. 9(9): 3298-3316, 2012.

748



750 **Figure 1. a) Location of the Metropolitan Area of Barcelona (AMB), b) Domain used to run the**
751 **UrbClim model. The blue line marks the border of the AMB, while the black line shows the**
752 **municipality of Barcelona. The numbers indicate the weather stations used to assess the LCZ-T**
753 **relationship.**

754

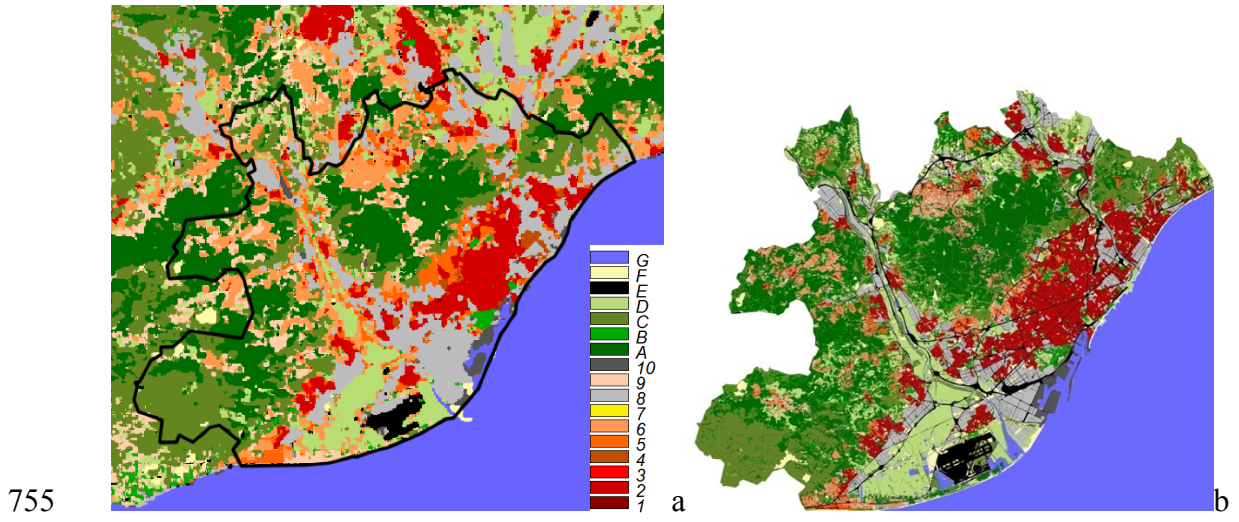
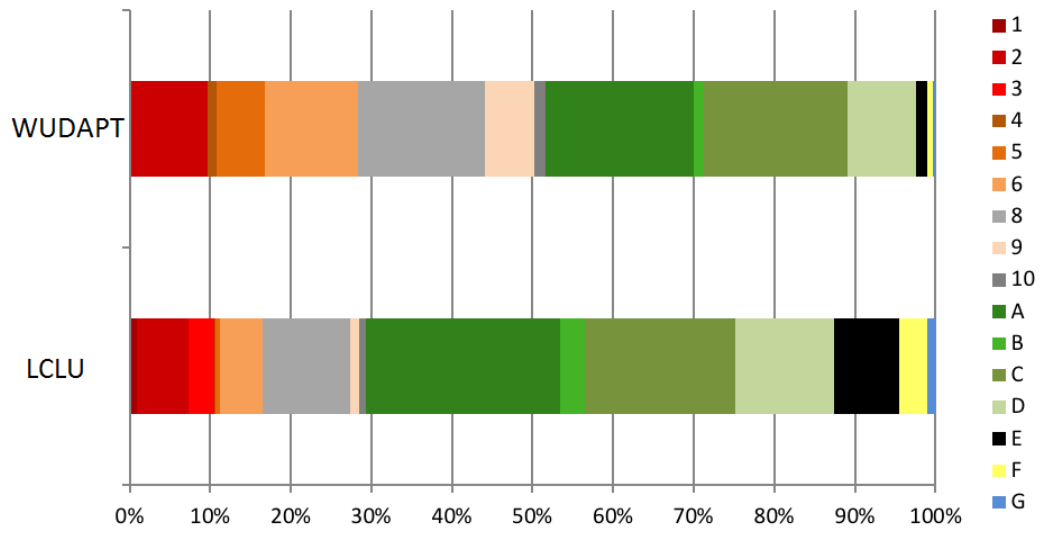


Figure 2. LCZ maps: a) WUDAPT method, b) LCLU method.



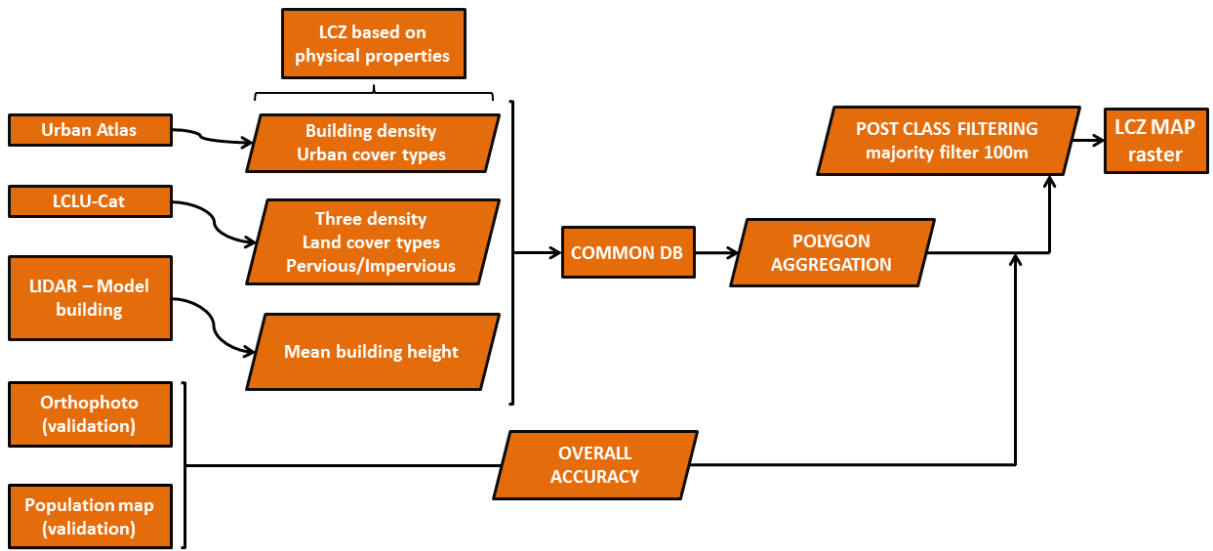
758

759 **Figure 3. Percentage of the area covered by each LCZ using WUDAPT and LCLU inside AMB.**

760

761

762

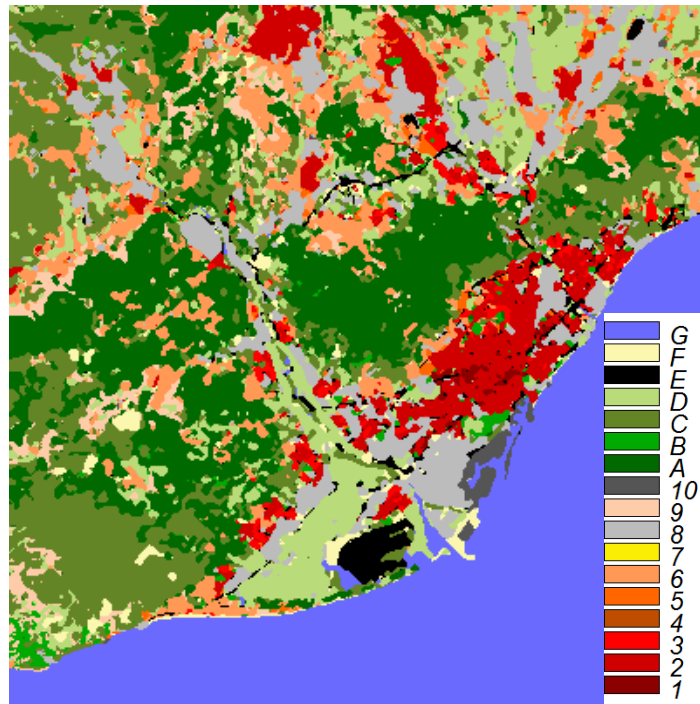


763

764

Figure 4. Workflow used to obtain the LCZ LCLU model.

765

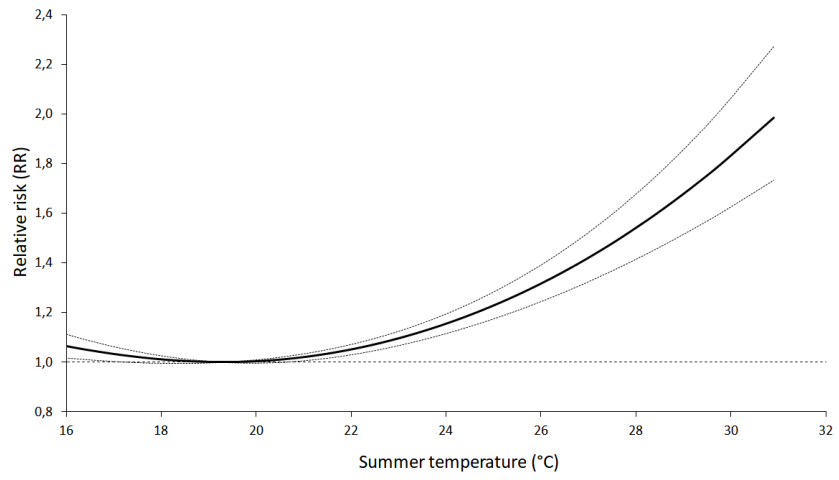


766

767

Figure 5. LCZ used in the UrbClim model based on workflow showed in Fig. 4.

768

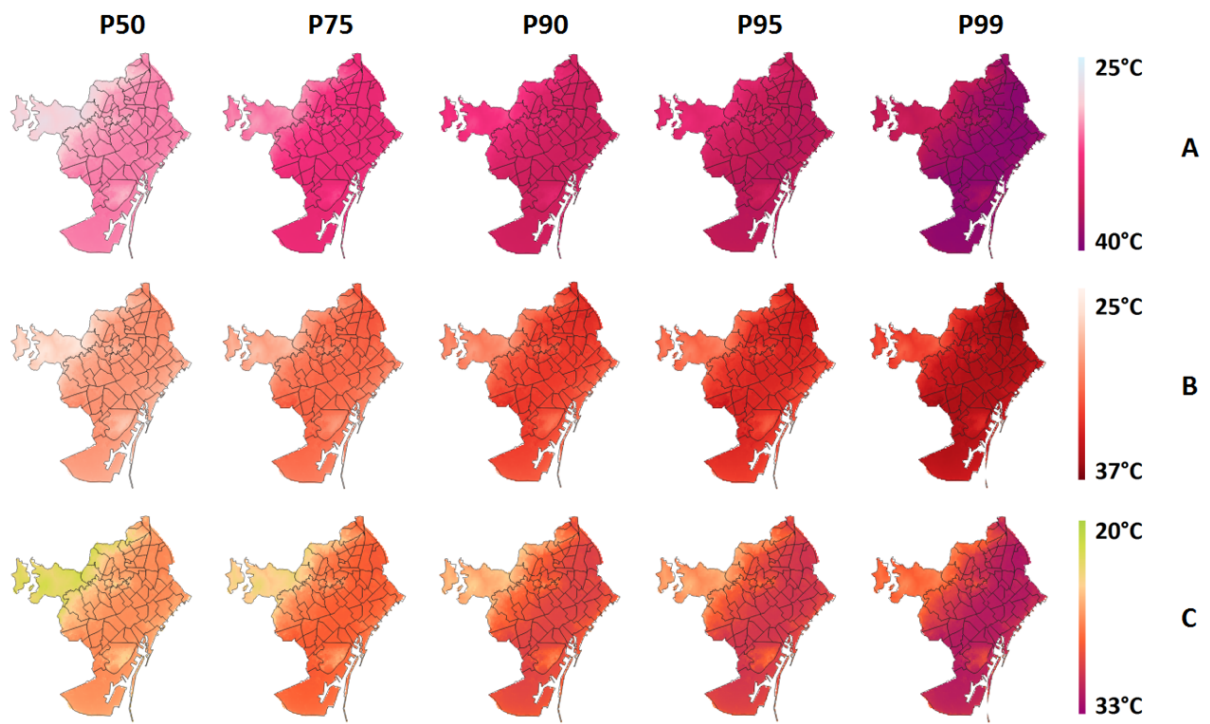


769

770 **Figure 6. Relative risk (RR) curve based on mortality due to summer daily temperature (JJA) in**
771 **Barcelona for the 1980 - 2015 period (Achebak et al., 2018).**

772

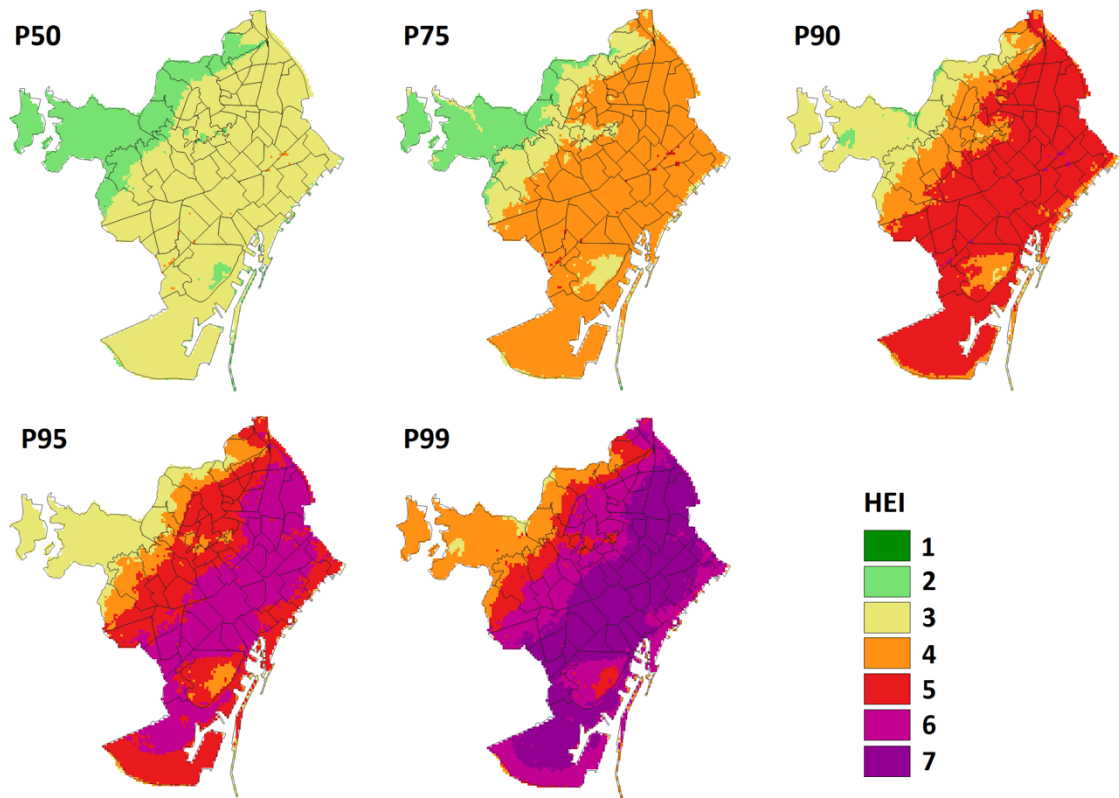
773



774

775 **Figure 7. Climatological conditions in summer modelled by UrbClim (1987 - 2016): A) HUMIDEX,**
 776 **B) Daily maximum temperature, C) Daily mean temperature, for the different distributions (P 50, P**
 777 **75, P 90, P 95 and P 99).**

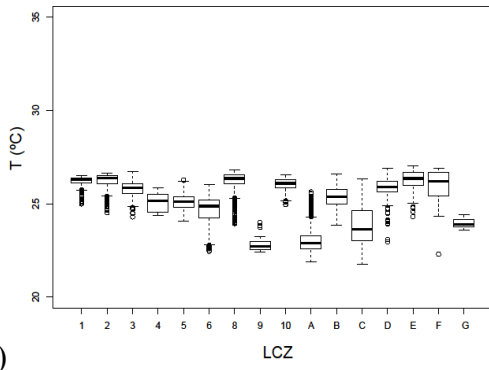
778



779

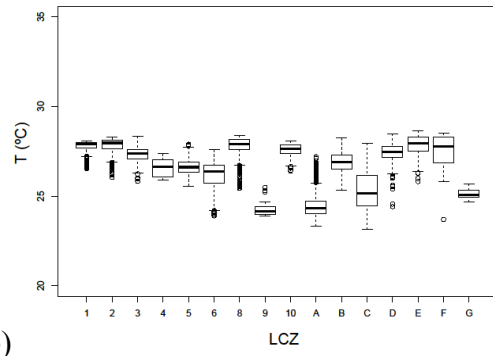
780 **Figure 8. Maps of HEI for the different probability distributions proposed (P 50, P 75, P 90, P 95**
 781 **and P 99).**

782

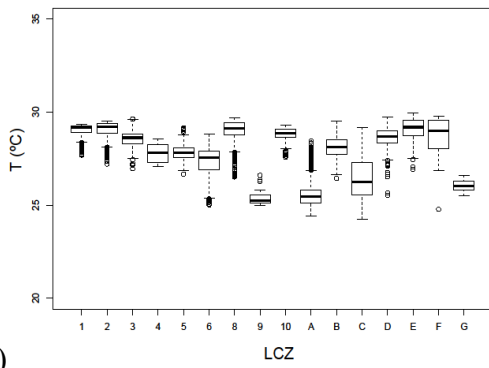


783

a)

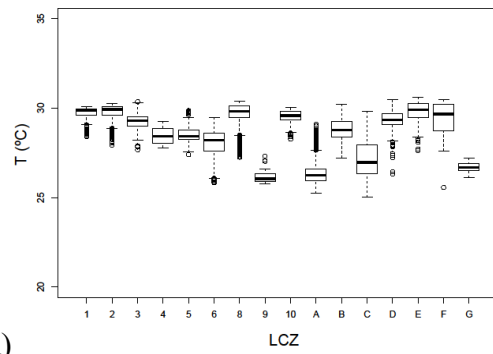


b)

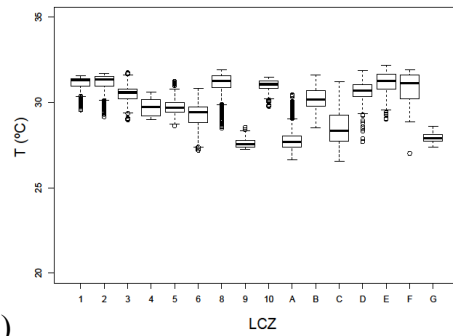


784

c)



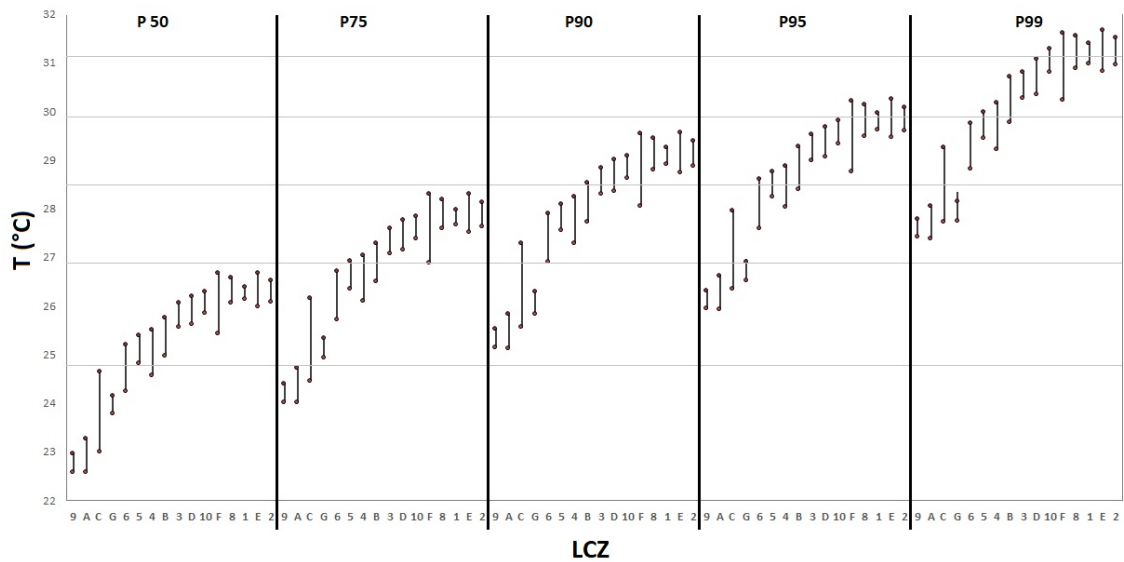
d)



785

e)

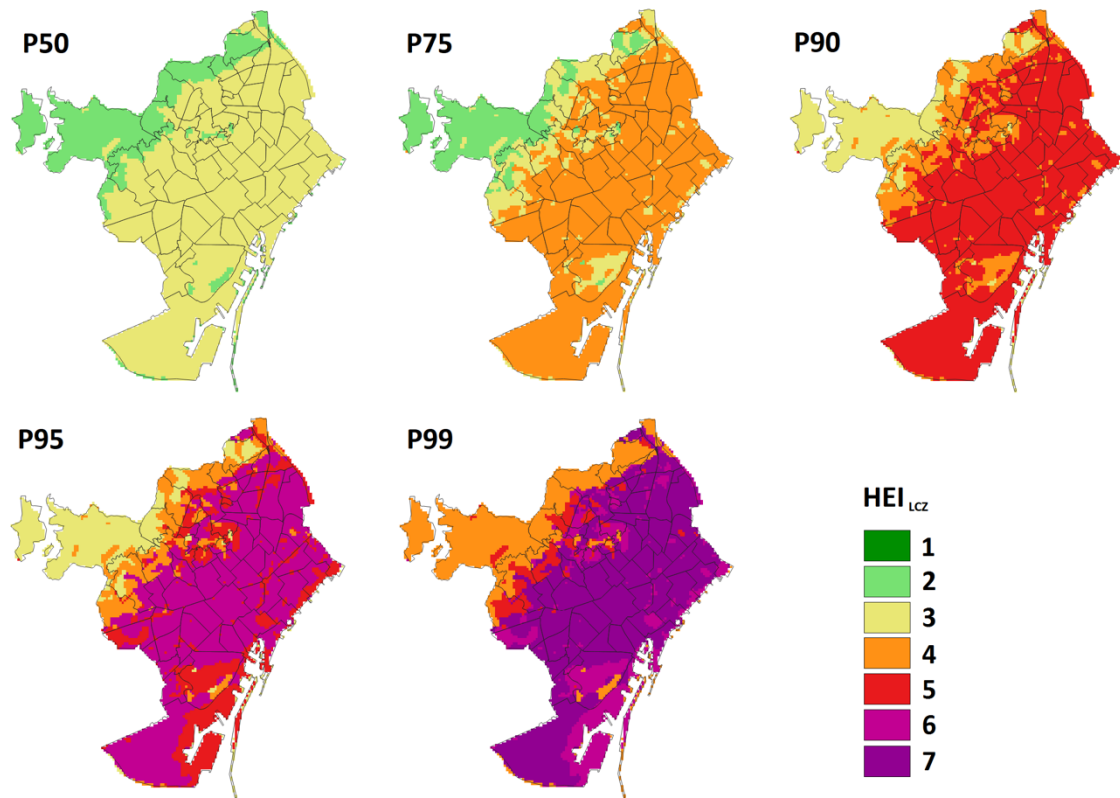
786 **Figure 9. Box plots for the thermal characterisation of the LCZ for different distributions: a) P 50,**
 787 **b) P 75, c) P 90, d) P 95 and e) P 99. (See S1 for LCZ features)**



788

789 **Figure 10. Characterisation of every LCZ with the daily mean temperature (1987 - 2016) for each**
 790 **probability scenario. Each bar shows P 25 and P 75, around the median for each LCZ (ordered**
 791 **from lowest to highest temperature). The grey horizontal lines are the different HEI scenarios (2 to**
 792 **7, lower to high).**

793



794

795 **Figure 11. Cartography of the heat exposure (HEI) in basis to thermal characterization of**
 796 **Barcelona by LCZs for different percentiles (LCZ - T) as shown in Table 3.**

797

798

Layer	Information	Spatial Resolution	Year	Format
Urban Atlas	20 categories of urban fabric	5 m	2010	Vector cartography
LCLU-Cat	241 categories	0.25 m	2010	Vector cartography
Building Heights	Height (m) (LIDAR)	0.5 m	2014	Vector cartography
Orthophoto	Mosaic of aerial photos	0.25 m	2016	Raster cartography
Population	Population by ages	62.5, 125, 250 m	2016	Vector cartography
LANDSAT 8	05/03/2015	30m	2015	Raster satellite

799 **Table 1. Vector and raster cartographic data and satellite images used to map the LCZ - LCLU and**
800 **LCZ - WUDAPT methods.**

801

802

803

ID	Weather Stations	Series	Years	LCZ	Z (m.a.s)	Variable
1	Raval	1997-2016	19	2	33	T daily
2	Zona Universitària	1997-2016	19	C	79	T daily
3	Fabra	1987-2016	29	A	411	T daily
4	Can Bruixa	1987-2015	28	2	61	T daily
5	Montjuïc	2004-2015	11	B	90	T daily

804 **Table 2. Weather stations in Barcelona used to assess the LCZ - T relationship based on daily mean**
805 **temperatures.**

806

807

808

809

810

811

812

RR	HEI	°C
1.0	1	18 -20
1.2	2	20 -24.7
1.4	3	24.7 -26.9
1.6	4	26.9 -28.5
1.8	5	28.5 -29.8
2.0	6	29.8 -31.1
>2.0	7	>31.1

813

Table 3. Temperature thresholds associated to heat exposure caused by high temperatures in basis

814

to figure 5. Heat Exposure Index (HEI) is assigned to each temperature range.

815

LCZ	P 50	P 75	P 90	P 95	P 99
1	0.301	0.325	0.349	0.363	0.419
2	0.356	0.379	0.396	0.401	0.475
3	0.450	0.468	0.486	0.489	0.552
4	0.528	0.530	0.535	0.522	0.569
5	0.467	0.488	0.504	0.500	0.541
6	0.821	0.841	0.872	0.843	0.804
8	0.465	0.499	0.527	0.531	0.580
9	0.456	0.474	0.461	0.441	0.379
10	0.319	0.338	0.339	0.338	0.322
A	0.686	0.712	0.725	0.705	0.649
B	0.554	0.580	0.603	0.616	0.641
C	1.090	1.128	1.168	1.128	1.088
D	0.550	0.572	0.596	0.586	0.612
E	0.530	0.561	0.599	0.595	0.678
F	0.848	0.918	0.960	0.955	0.978
G	0.224	0.265	0.297	0.294	0.289

816

Table 4. Standard deviations for the LCZs for the different percentiles of temperature.

817

	DIST	OB	UC	LCZ-T	Δ OB-UC	Δ OB-LCZ-T
1-Raval (LCZ 2)	P50	25.6	26.1	26.1	0.5	0.5
	P75	26.8	27.6	27.6	0.8	0.8
	P90	27.8	28.9	28.9	1.1	1.1
	P95	28.5	29.6	29.6	1.1	1.1
	P99	30.2	31.1	30.9	0.9	0.7
2-ZU (LCZ C)	P50	24.5	24.7	24.6	0.2	0.1
	P75	25.8	26.2	26.2	0.4	0.4
	P90	26.6	27.3	27.3	0.7	0.7
	P95	27.2	28.1	27.9	0.9	0.7
	P99	28.5	29.5	29.2	1	0.7
3-Fabra (LCZ A)	P50	23.1	23.1	22.9	0	-0.2
	P75	24.6	24.7	24.3	0.1	-0.3
	P90	25.9	25.8	25.5	-0.1	-0.4
	P95	26.5	26.6	26.2	0.1	-0.3
	P99	27.3	27.5	27.7	0.2	0.4
4-C. Bruixa (LCZ B)	P50	25.2	26.1	25.4	0.9	0.2
	P75	26.8	27.6	26.9	0.8	0.1
	P90	27.9	28.9	28.1	1	0.2
	P95	28.6	29.6	28.8	1	0.2
	P99	30	30.9	30.2	0.9	0.2
5-Monjuïc (LCZ B)	P50	24.8	25.2	25.0	0.4	0.2
	P75	26.3	26.8	26.5	0.5	0.2
	P90	27.3	28	27.7	0.7	0.4
	P95	27.8	28.6	28.4	0.8	0.6
	P99	29.1	30.1	29.8	1	0.7

819 **Table 5. Temperature for each distribution/scenario (DIST) and weather station observed (OB),**
820 **modelled by UrbClim (UC) and estimated from the distribution of temperature (the mean value is**
821 **taken) for each LCZ (LCZ-T). The difference (Δ) between them is also showed. All the values are**
822 **expressed in ° C.**

MODEL	P50	P75	P90	P95	P99
Underestimate	284	671	1711	2789	2289
Good	9687	8762	8175	6316	6823
Overestimate	247	785	332	1103	1106
% correct	95	86	80	62	67
RMSE	0.23	0.38	0.45	0.62	0.58

824 **Table 6. Number of pixels where the HEI obtained through the LCZ-T model (Figure 11)**
825 **underestimate, overestimate or coincide with the HEI provided by the Urban Climate Model**
826 **(Figure 6) for the different scenarios. Percentage of coincidences and RMSE are also showed.**

827

828